

# Measurement, Characterization, and Modeling of LoRa Technology in Multifloor Buildings

Weitao Xu<sup>ID</sup>, Member, IEEE, Jun Young Kim<sup>ID</sup>, Graduate Student Member, IEEE, Walter Huang, Salil S. Kanhere<sup>ID</sup>, Sanjay K. Jha, Senior Member, IEEE, and Wen Hu, Senior Member, IEEE

**Abstract**—In recent years, we have witnessed the rapid development of the long range (LoRa) technology, together with extensive studies trying to understand its performance in various application settings. In contrast to measurements performed in large outdoor areas, a limited number of attempts have been made to understand the characterization and performance of the LoRa technology in indoor environments. In this article, we present a comprehensive study of the LoRa technology in multifloor buildings. Specifically, we investigate the large-scale fading characteristic, temporal fading characteristic, coverage, and energy consumption of the LoRa technology in four different types of buildings. Moreover, we find that the energy consumption using different parameter settings can vary up to 145 times. These results indicate the importance of parameter selection and enabling the LoRa adaptive data rate feature in energy-limited applications. We hope the results in this article can help both academia and industry understand the performance of the LoRa technology in multifloor buildings to facilitate developing practical indoor applications.

**Index Terms**—Field study, indoor propagation, long range (LoRa), smart building, temporal fading (TF).

## I. INTRODUCTION

THE Internet of Things (IoT) brings the promise of a world comprising smart cities, smart buildings, and smart homes to improve every aspect of our lifestyle. The rapid development of various IoT applications has created the requirement of new wireless technologies that can provide cost-effective large area coverage. Low-power wide-area network (LPWAN) communication technologies have recently emerged as a viable alternative to cellular and mesh networks to fulfill the vast requirements. LPWANs are designed to fill the gap between short-range, high-bandwidth (BW) networks (e.g., Bluetooth, WiFi, and ZigBee), and cellular networks (e.g., GSM and LTE) [1]. Many LPWANs applications are

Manuscript received December 28, 2018; revised April 18, 2019 and September 13, 2019; accepted September 22, 2019. Date of publication October 11, 2019; date of current version January 10, 2020. This work was supported by the Australian Research Council Linkage Project under Grant LP160101260. (*Corresponding author: Weitao Xu*)

W. Xu, S. S. Kanhere, and S. K. Jha are with the School of Computer Science and Engineering, University of New South Wales, Sydney, NSW 2032, Australia (e-mail: w.t.xu@unsw.edu.au; salil.kanhere@unsw.edu.au; sanjay.jha@unsw.edu.au).

J. Y. Kim and W. Huang are with WBS Technology, Sydney, NSW 2128, Australia (e-mail: jun.kim@wbstech.com.au; walter@wbstech.com.au).

W. Hu is with the School of Computer Science and Engineering, University of New South Wales, Sydney, NSW 2032, Australia, and also with WBS Technology, Sydney, NSW 2128, Australia (e-mail: wen.hu@unsw.edu.au).

Digital Object Identifier 10.1109/JIOT.2019.2946900

proving its cost efficiency and large-scale IoT application suitability. Examples of such LPWAN technologies include long range (LoRa) [2], Sigfox [3], and NB-IoT [4]. Among these competing LPWAN technologies, LoRa is attracting attention primarily since it offers affordable connectivity to the low-power devices distributed over large geographical areas.

Despite its young age, LoRa has grown rapidly and drawn wide attention in the past few years. Extensive research has already been carried out in the outdoor environment to understand the performance of the LoRa technology [5]–[9]. It is reported that the communication range can be up to 15 km with over 60% delivery rate in line-of-sight (LOS) conditions in rural areas [5]. Apart from the applications in wide areas, such as smart city and smart traffic, the LoRa technology can also become the enabler for new applications in the indoor environment, such as gas meter monitoring, home automation, and smart buildings. However, according to our survey, the performance evaluation of LoRa in the indoor environment either uses a limited number of nodes [5] or focuses on only few metrics, such as received signal strength indicator (RSSI) and signal-to-noise ratio (SNR) [1]. Few attempts have been made to comprehensively study the propagation, characterization, and performance of the LoRa technology in multifloor buildings, especially buildings with multistory basements.

Our industry partner WBS Technology<sup>1</sup> is a smart building solution provider in Australia. We have implemented and deployed a LoRa-based smart building network in nine production smart building of different types. It is known that different buildings have different communication conditions because of the difference in size, shape, and structure. In order to make sure the designed LoRa network works at its optimal communication mode, it is crucial to understand the characteristics and performance of the LoRa in different environments. Although the radio propagation model and the temporal fading (TF) model have been extensively studied previously, these models are not intended for one particular communication technology. Many radio propagation models have been proposed in the literature, such as Okumura–Hata [10], one-slope model [11], and ITU model [12]. However, it is known that the propagation and performance of wireless communication is affected by a variety of factors, such as distance, frequency band, walls and floors, geography and terrains, etc. For this reason, extensive works have been done to

<sup>1</sup><https://wbstech.com.au/>



Fig. 1. Experimental setup. (a) LoRa mote. (b) Office building. (c) Residential building. (d) Car park. (e) Warehouse. Floor plan of (f) level 4 and (g) ground level.

understand the characteristics of different communication technologies, such as WiFi [13], IEEE 802.15.4 [14], 5G [15], etc. Correspondingly, it is imperative to conduct a detailed study to investigate the characteristics of recently developed LoRa technology. Unfortunately, some recent works only focus on one aspect of LoRa, such as radio propagation or coverage (see related work for more details). To this end, we perform a detailed study to understand the propagation, characteristics, performance, and energy consumption of the LoRa technology in different multifloor buildings. In particular, we deployed a LoRa testbed which consists of ten LoRa nodes in one of the testing buildings. To the best of our knowledge, this is the first attempt to comprehensively investigate the large-scale fading (LSF), TF, coverage, and energy consumption of the LoRa technology in different multifloor buildings. With the help of the results in this article, the LoRa network deployed in nine different buildings has successfully run for over six months (for more details please visit the homepage of WBS Technology). We also hope that these results can provide insights for other companies who are interested in using LoRa in their applications.

The remainder of this article is organized as follows. Section II describes the experimental setup, and Section III presents the measurement methodology. Followed by that, the results of LSF characterization, TF characterization, and coverage experiment are presented in Sections IV–VI, respectively. Finally, Section VII discusses the related work, and Section VIII concludes this article.

## II. MEASUREMENT CONFIGURATION

### A. Experimental Environment

As the products of WBS Technology can be deployed in different types of buildings, we conduct the study in four different types of buildings: 1) an office building; 2) a residential

TABLE I  
DETAILS OF EXPERIMENTAL ENVIRONMENT

Building No	Type	Size ( $m^3$ )	No. of Floors	No. of Basement
1	Office Building	$20 \times 36 \times 27$	6	1
2	Residential Building	$45 \times 55 \times 22$	5	3
3	Car park	$65 \times 70 \times 18$	5	0
4	Warehouse	$16 \times 60 \times 10$	1	0

building; 3) a car park; and 4) a warehouse. Table I summarizes the details of these buildings and Fig. 1 provides some pictures of these buildings. The office building is a reinforced concrete building, which is located on a university campus. The building has six floors and one basement. The floor plan of level 4 and ground level is shown in Fig. 1(f) and (g), respectively. The residential building has five floors and three basements while the car park has five aboveground levels. The warehouse has only one level but many metal shelves and boxes as shown in Fig. 1(e).

### B. Measurement Apparatus

The hardware platform used in the study is Multitech mDot<sup>2</sup> which comprises a LoRa wireless chip (SX1272), an ARM processor, and the LoRaWAN protocol stack. For the office building, we have deployed a LoRa testbed which consists of ten LoRa motes. The LoRa mote is connected to a Raspberry Pi as shown in Fig. 1(a). The Raspberry Pi will collect log data sent from LoRa mote through USB port, then transmit the data to a local server via Ethernet. The LoRa motes are evenly distributed in the building. Each mDot is equipped with an omnidirectional vertically polarized antenna with a gain of 3 dBi.

For the rest of the testing buildings, we use two mDots to collect data: they are configured as transmitter (Tx) and receiver (Rx). The RSSI reported by mDot is just an indication

<sup>2</sup><https://www.multitech.com/brands/multiconnect-mdot>

TABLE II  
PARAMETER SETTINGS IN COVERAGE EVALUATION

BW (Khz)	Center frequency (Mhz)	SF	Tx power (dBm)
500	915	7	20
250	919	8	
125	923	9	
	928	10	

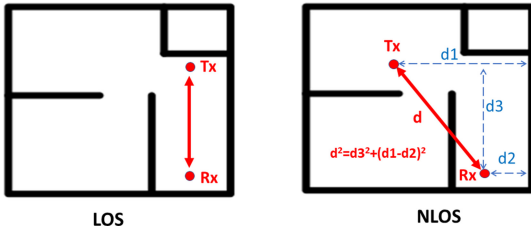


Fig. 2. Distance measure.

(represented by a number) of the power level being received by the antenna. Thus, a calibration of the LoRa mote using the spectrum analyzer has been performed to determine the shift constant between the RSSI and the radio-frequency (RF) power. The method to determine the relation between the RSSI values and the real radio power is the same as [16]. A constant shift of 2 dB has been found between the RSSI reported by mDot and the RF power measured by the spectrum analyzer. For all the experiments in this article, the parameters of the LoRa module are set to the default values in Table II unless otherwise stated.

### III. MEASUREMENT METHODOLOGY

#### A. Characterization of Large-Scale Fading

LSF is defined as the variability of received power with distance. The parameter characterizing LSF is the path loss (PL).

1) *Measurement Method:* To determine the LSF properties of LoRa in the indoor environment, two LoRa nodes are used in the data collection phase: Tx and Rx. Tx is placed at a fixed position which is 1.5 m above the floor. Rx is placed at different locations to collect RSSI at different distances. The distance between Tx and Rx is measured by a laser meter measurer. When there is LOS between Tx and Rx, the distance can be measured directly using a laser meter measurer. When there is NLOS between Tx and Rx, we calculate the distance of Tx and Rx to a fixed point, then the distance between Tx and Rx can be measured by the Pythagorean theorem as depicted in Fig. 2.

For each building, the measurement is conducted in three different LSF scenarios. The LSF scenarios are divided by whether or not LOS between Tx and Rx exists, and by the number of floor between them. LSF scenario categories are specified as follows. Due to space limitations, we do not plot the floor plan of each building in this article. Instead, we only plot the floor plan and experimental settings of the office building for illustrative purposes.

1) *LSF Scenario 1 (LOS Path):* LOS between Tx and Rx exists at every point along the path. For example, in the office building, the path is along a straight aisle on the fourth floor as shown in Fig. 1(f) (blue line).

2) *LSF Scenario 2 [Obstructed LOS Path (OBS) on the Same Level]:* LOS between Tx and Rx is occasionally blocked between Tx and Rx. For example, in the office building, the path is along an aisle other than the aisle where Tx is located as shown in Fig. 1(f) (green line).

3) *LSF Scenario 3 [None-LOS (NLOS) Path on Different Levels]:* There is no LOS between Tx and Rx. In the testing buildings which has more than one floor (i.e., office building, residential building, and car park), the researcher walks along an aisle at different levels other than the level where Tx is located. The experiment in the warehouse is conducted on the same floor as it has one level only. In this case, there are multiple shelves between Tx and Rx to make sure there is no LOS between them.

2) *Path Loss Model:* LSF characteristics of the indoor radio channel are determined by measurements of PL. The PL model can be used in the link budget calculation. A distance-dependent PL model (also called one-slope model) has been demonstrated to perform well in indoor environments [17], [18]. According to this empirical model, the relationship between  $PL(d)$  in decibels and distance  $d$  in m between Tx and Rx can be expressed as follows:

$$PL(d) = PL(d_0) + 10n \log\left(\frac{d}{d_0}\right) + X_\sigma \quad (1)$$

where  $PL(d_0)$  is the PL at reference distance (1 m in our measurement),  $n$  is the PL exponent,  $d$  is the separation distance between TX and RX, and  $X_\sigma$  is a zero-mean Gaussian distributed variable (in decibels) with standard deviation  $\sigma$ , also in decibels.

In this experiment, PL samples are gathered up to a distance of 70 m between Tx and Rx. The parameters  $PL(d_0)$  and  $n$  are obtained by fitting the PL model to the measured PL samples in a least-squares sense. Following [11] and [19], the intercept  $PL(d_0)$  can be determined in two ways.

- 1) *Nonfixed Intercept:* The intercept  $PL(d_0)$  is considered as a separate outcome of the least-squares fit.
- 2) *Fixed Intercept:* The intercept  $PL(d_0)$  is chosen fixed and equal to PL at reference distance  $d_0$  which is 1 m in our measurement.

In this article, a comparison between the nonfixed and fixed intercept method is made to investigate which approach provides a better fit to measurement data.

3) *Shadowing Effect:* To characterize shadowing properties of the indoor environment, deviations  $X_\sigma$  in decibels between the PL model with estimated parameters and the measured PL samples are calculated by  $X_i = PL(d_i) - PL_i$ , where  $PL_i$  is the  $i$ th PL sample measured at distance  $d_i$  and  $PL(d_i)$  is the PL value predicted by the empirical model at distance  $d_i$ . It is shown that shadow fading samples  $X_i$  closely follow a lognormal distribution with median equal to 0 dB [17], [18]. For a particular path, shadow fading samples  $X_i$  are calculated with respect to the PL model fitted to the measurements collected along that path. Suppose we obtain  $N$  shadow fading samples from a measurement track, the normalized autocorrelation function  $R_{xx}(i)$  associated with that track is calculated as:  $R_{xx}(i) = [(\sum_{p=1}^{N-i} X_p X_{p+i}) / (\sum_{q=1}^N X_q^2)]$ .

For each track, we calculate the autocorrelation function to analyze the shadowing characteristics. Particularly, we also calculate the decorrelation distance which is defined as the distance to which the normalized autocorrelation drops below 0.1. This definition is commonly used, as autocorrelation can often be modeled as exponentially decaying with distance [20].

### B. Characterization of Temporal Fading

TF is defined as the variability of received signal strength over time at a fixed location in the propagation environment. Previous studies show fading statistics, which follows a Rician distribution when a dominant multipath component (e.g., LOS component) exists [16], [21]. Therefore, we model the measured TF samples and compare with the theoretical Rician distribution.

1) *Measurement Method*: Different from LSF, the TF is not determined by stationary physical characteristics, such as LOS or NLOS. Instead, it is caused by the movement of persons in the multipath environment. To determine TF properties of the LoRa technology in the multifloor building, two different TF scenarios are considered.

1) *TF Scenario 1*: Both Tx and Rx are put at a fixed location on the same floor. As an example, the positions of Tx and Rx are shown in Fig. 1(f).

2) *TF Scenario 2*: Tx and Rx are located at different levels. For example, in the office building, Tx remains at level 4 while Rx is put at a fixed position on the ground level as shown in Fig. 1(g). In the warehouse, Tx and Rx are separated by a number of shelves.

In each scenario, the received signal strength is recorded in a time span of 1 h, at a rate of approximately 30 samples/s. After data collection, the median received power  $P_{\text{median}}$  in dBm is removed from the received power samples  $P_i$  as  $Y_i = P_i - P_{\text{median}}$ . The samples  $Y_i$  will be compared with the Rician distribution to analyze the TF characteristics. The Rician distribution is often described in terms of a parameter  $K$  (Rician factor), which is defined as the ratio between the power received via the dominant path and the power contribution of the obstructed paths [22]. The parameter  $K$  is given by  $K = A^2/2b^2$  or in terms of dB  $K = 10 \log(A^2/(2b^2))$ , where  $A^2$  is the energy of the dominant path and  $2b^2$  is the energy of the diffuse part of the received signal [22]. From the definition of the Rician  $K$ -factor, low  $K$ -factor indicates the large motion (i.e., large  $b$ ) within the wireless propagation environment that disturbs the received power profile over time, while large  $K$ -factor reveals a low movement in the environment. To estimate the  $K$ -factor, two distinct methods are used in this article.

- 1) *Moment-Based Estimator*: To estimate the  $K$ -factor, the method of moments proposed in [22] is used. This method provides a simple parameter estimator based on the variance and the mean of the received signal strength.
- 2) *Curve Fitting*: To estimate the  $K$ -factor, the empirical cumulative distribution function (CDF) is constructed and compared to a Rician distribution with zero median in decibels using a least-squares curve fitting technique.

TABLE III  
NONFIXED METHOD VERSUS FIXED METHOD

Building	LSF Scenario	Non-fixed Intercept			Fixed Intercept		
		PL( $d_0$ ) [dB]	n [-]	$\sigma$ [dB]	PL( $d_0$ ) [dB]	n [-]	$\sigma$ [dB]
1	1-LOS	38	2.17	4.99	37	2.35	5.04
	2-OBS	39	2.43	5.17	37	2.54	5.18
	3-NLOS	45	6.03	5.88	37	8.2	5.95
	Average	<b>40.7</b>	<b>3.54</b>	<b>5.34</b>	<b>37</b>	<b>4.36</b>	<b>5.38</b>
2	1-LOS	38	2.31	4.87	37	2.35	4.97
	2-OBS	39	2.05	4.62	37	4.71	4.84
	3-NLOS	42	5.64	5.01	37	5.8	5.31
	Average	<b>39</b>	<b>3.33</b>	<b>4.83</b>	<b>37</b>	<b>4.29</b>	<b>5.04</b>
3	1-LOS	38	1.52	4.7	36	1.74	4.8
	2-OBS	40	1.87	4.57	36	1.94	4.79
	3-NLOS	46	8.4	5.32	36	8.7	5.64
	Average	<b>41.3</b>	<b>3.93</b>	<b>4.86</b>	<b>36</b>	<b>4.13</b>	<b>5.07</b>
4	1-LOS	42	1.7	5.23	36	2.43	5.85
	2-OBS	43	1.74	5.11	36	2.27	5.47
	3-NLOS	44	3.8	5.49	36	4.62	5.92
	Average	<b>42.7</b>	<b>2.41</b>	<b>5.27</b>	<b>36</b>	<b>3.11</b>	<b>5.74</b>

In this article, the moment-based and the curve fitting method will be compared to determine how well TF fits Rician distribution. The results of TF are presented in Section V.

### C. Coverage Evaluation

In this set of experiments, we aim to evaluate the coverage of the LoRa technology in multifloor buildings using different parameter settings. Specifically, we will focus on the packet reception rate (PRR) as it is an important metric for wireless sensor network. The parameters investigated in this article include data rate, BW, center frequency, and spread factor (SF). During the experiment, we put Tx at the top floor, and change the position of Rx from the top floor to the lowest floor to investigate the changes in PRR. For each floor, we choose ten evenly distributed points to collect data. For each point, Rx keeps receiving packets sent from Tx for 30 min. The PRR of each floor is obtained by averaging the results of ten points. As the warehouse has only one level, we do not conduct an experiment in the warehouse. Table II lists all the parameter values tested in this article. The parameter values marked in bold are called default values.

## IV. LARGE-SCALE FADING RESULTS

### A. Path Loss Per LSF Scenario

The parameters of the one-slope model in Section III-A2 are determined separately for each LSF scenario. Table III shows the PL( $d_0$ ) at reference distance  $d_0 = 1$  m and the PL exponent  $n$ , as well as the standard deviation  $\sigma$  of the samples. Distinction has been made between one-slope models with nonfixed and fixed intercept PL( $d_0$ ). In the following, the results of the PL measurements are discussed.

1) *Comparison Between Nonfixed and Fixed Intercept Models*: The results of different buildings and different methods are summarized in Table III. From Table III, we find some regular patterns. First, for all the buildings, the intercept PL( $d_0$ ) of the nonfixed intercept model is consistently larger than that of the fixed intercept model. Second, smaller PL exponents  $n$  are obtained with the nonfixed intercept model in comparison with the fixed intercept model. Third, the standard deviations  $\sigma$  for nonfixed intercept and fixed intercept

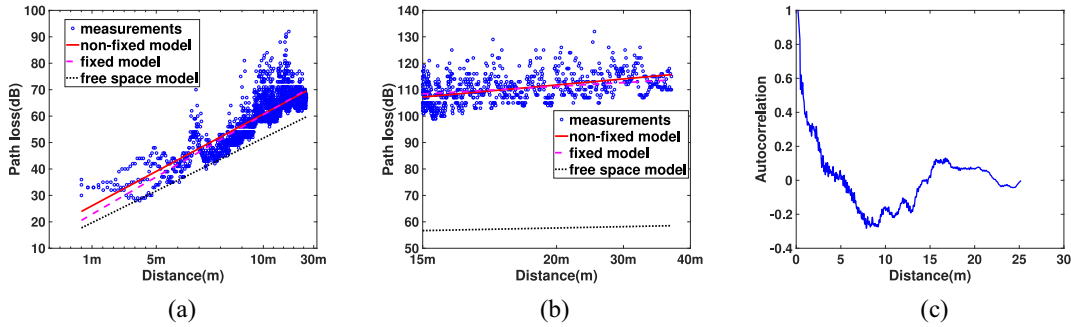


Fig. 3. Evaluation results of LSF. (a) LSF scenario 1. (b) LSF scenario 3 (ground level). (c) Decorrelation distance.

match well, although they are consistently somewhat larger for the fixed intercept method.

Based on the smaller standard deviation between the model and real measurements, we can draw the conclusion that the use of a PL model with a nonfixed intercept is superior to using a fixed-intercept model. This is due to the following two reasons: first, it is noteworthy that the difference in  $\text{PL}(d_0)$  between the nonfixed intercept and the fixed intercept models in Table III can occasionally be as high as 8 dB. Therefore, free-space propagation at reference distance  $d_0$  (assumed for fixed intercept models) can hardly be assumed for our measurements. This is probably caused by the multipath effect of the indoor environment. Free-space propagation can usually only be assumed in spacious areas free of immediate obstructions, in contrast to our measurement configuration where Tx and Rx are obstructed by soft partitions and floors.

Second, it is generally accepted in the literature that shadow fading samples  $X_i$  are log-normally distributed. To ascertain log-normality, a Kolmogorov–Smirnov (K–S) goodness-of-fit test has been performed on the shadow fading samples of the one-slope models provided in Table III. For the K–S test, the empirical CDF of shadow fading samples is compared to a log-normal CDF with zero median in decibels and a standard deviation  $\sigma$  of the corresponding model. For the three LSF topographies in Table III, the nonfixed intercept one-slope models passed the K–S test at  $\alpha = 0.05$  level of significance, whereas only 3 out of 12 fixed intercept models passed the same test. This indicates that median PL is most accurately specified by a PL model with a nonfixed intercept. Moreover, standard deviations  $\sigma$  in Table III are somewhat smaller for the nonfixed intercept in comparison with fixed intercept, showing that a nonfixed intercept one-slope model provides a better fit to experimental path-loss data.

As an example, Fig. 3(a) and (b) shows the measured path-loss samples and the predicted model of LSF scenario 1 and ground level of LSF scenario 3, respectively. Also shown in the figure is the free-space PL at 915 MHz. As expected, the PL predicted by both nonfixed intercept and fixed intercept is higher than the free-space PL.

In Table III, we can also observe building-to-building path-loss variations. However, building-to-building variation is not large. For example, in terms of LSF scenario 1, the PL exponents  $n$  vary only from 1.54 to 2.43 among different types of buildings. This is mainly because the construction details of

all measured buildings are similar (e.g., concrete floors and walls).

**2) Soft Partition and Concrete Wall Attenuation Factor Model:** In the previous section, the PL in multifloored environment is predicted by a model that includes distance only. However, from Table III, it can be seen that the PL exponent  $n$  changes greatly in different LSF scenarios and the standard deviation  $\sigma$  can be as high as 5.74 dB. These parameters may be used in the model for a first-order prediction of mean signal strength when only distance but no other information such as the number of floors is known, but is clearly unsatisfactory for site layout or capacity prediction.

There are often obstructions between Tx and Rx, such as soft partitions, walls, and floors. In order to build a more accurate propagation model, we need to consider the PL effects of these obstructions. In [23], this is achieved by including the attenuation factor of floor, soft partition, and wall in the prediction model. For simplicity, we assume that any kind of concrete support column that wholly or partially blocks the direct path between Tx and Rx is labeled as a concrete wall. Let  $p$  and  $q$  be the number of soft partition and concrete wall between Tx and Rx, respectively. Then PL predicted by the attenuation factor model (AF model) is given by

$$\text{PL}(d) = \text{PL}(d_0) + 10n \log\left(\frac{d}{d_0}\right) + \text{FAF}[dB] + p * \text{AF}_{\text{partition}}[dB] + q * \text{AF}_{\text{wall}}[dB] \quad (2)$$

where FAF is the floor attenuation factor, and  $\text{AF}_{\text{partition}}$  and  $\text{AF}_{\text{wall}}$  are the attenuation factor of one soft partition and concrete wall, respectively. To obtain a more precise PL model, we conduct a drive test to calculate the attenuation factors of different types of obstructions in the test building. Specifically, we first measure PL when Tx and Rx are separated by 2 m, then we calculate PL when Tx and Rx is separated by the same distance but with an obstruction between them (e.g., wall and soft partition). The difference of PL between these two tests is regarded as the attenuation factor of this type of obstruction. For each type of obstruction, we repeat the test for multiple times at different locations of the building, and the final result is obtained by calculating the mean of these tests. It is worth mentioning that the attenuation factor is only calculated in the office building.

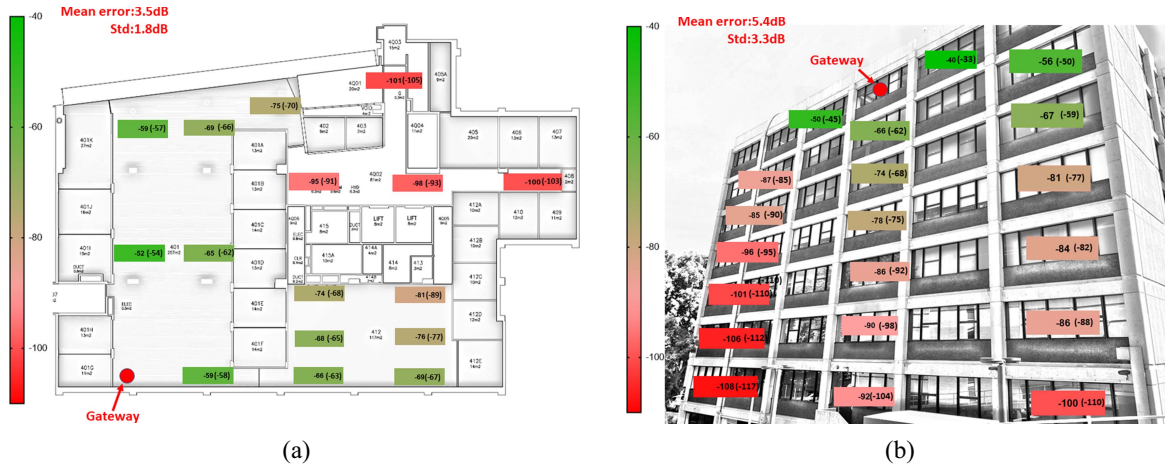


Fig. 4. Accuracy of the PL model (the values in the parenthesis are predicted value). (a) Same floor. (b) Different floor.

TABLE IV  
ATTENUATION FACTORS

Obstruction	AF (dB)	Previous Studies		
		[23](914Mhz)	[24](2.4Ghz)	[24](2.4Ghz)
1 floor	21.7	12.9	16	21
2 floors	25.9	18.7	27	33
3 floors	27.2	24.4	31	40
4 floors	50.8	27	-	-
Concrete wall	2.2	-	-	2.73
Glass	2.04	-	-	4.5
Wooden door	2.11	-	-	2.67
Soft partition board	2.5	-	-	2.3 (2.5Ghz [27])

The attenuation factors of different types of obstruction are summarized in Table IV. For comparison purpose, we also list the attenuation factors reported in the literature. We can see that the FAF varies greatly in different buildings with varied frequencies. This result indicates that a site-specific PL model is required because of the different construction materials and layout as well as many other factors. However, the attenuation factors of the concrete wall, wooden door, and soft partition in our measurements are similar to those reported in the previous studies. The attenuation factor of glass measured in this article (2.04 dB) is different from the previous results (4.5 dB). It is probably because the thickness of glass in [24] is different from that in our experimental building which is about 2 cm. It is also interesting to note that the average FAF is not a linear function of the number of floors between Tx and Rx as also found in [25] and [26]. It is possible that different floors cause different amounts of PL, and there may be other factors such as multipath reflections from surrounding buildings that affect the PL. With the knowledge of attenuation factors, we recalculate the PL model using curve fitting with the nonfixed intercept method. In order to demonstrate the benefits of the AF model, in LSF scenario 3, we put TX on level 4 and change the position of RX from level 4 to ground floor level by level. From the results in Table X, we find that the standard deviation reduces from 5.84 to 4.21 which indicates that the AF model is more accurate.

Based on the above results, we build a model for PL estimation in multifloor buildings. As the model in (2) is trained from the office building, we test the accuracy of the model

TABLE V  
COMPARISON RESULTS

LSF scenario	Level	$\sigma$ [dB]	$\sigma$ [dB]
		General model	AF model
1(LOS)	4	-	-
2(OBS)	4	5.17	4.12
	3	4.88	3.76
3(NLOS)	2	5.7	4.11
	1	6.61	4.32
	Ground floor	6.85	4.77
All	-	5.84	4.21

in the office building. In this test, we consider two scenarios: 1) same floor and 2) different floors. For each scenario, the gateway is placed at a fixed position as shown in Fig. 4. Then we place a LoRa node at multiple locations to record the true RSSI measurement. Meanwhile, for each location, we predict the RSSI value by the model in (2). The results of the same floor and different floors are shown in Fig. 4(a) and (b), respectively. We can see that the mean error in two scenarios is as low as 3.5 and 5.4 dB which indicates that the model can predict PL in this building with high accuracy.

### B. Shadowing Characteristics

The spatial correlation characteristics of shadow fading are investigated by means of calculating the normalized autocorrelation function. To this end, the one-slope models are fitted to the PL data of each measurement track separately. A non-fixed intercept is used in the determination of the one-slope models' parameters. As stated above, the model with non-fixed intercept provides a more accurate representation of the median PL. Then, we calculate the normalized autocorrelation function  $RXX(m)$  as mentioned in Section III-A3.

We now present the results of shadowing characteristics as the steps in Section III-A3. An example of the normalized autocorrelation versus distance for one measurement track is shown in Fig. 3(c). We can see a rapid decrease in autocorrelation with distance. This reinforces the popular assertion that shadow fading autocorrelation decays exponentially with distance, as reported in [19] and [20]. Decorrelation distances,

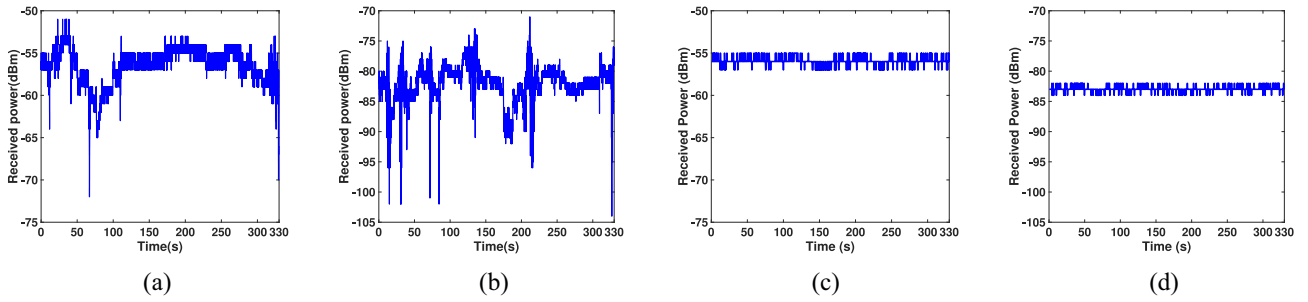


Fig. 5. TF measurement. (a) TF scenario 1. (b) TF scenario 2. (c) TF scenario 1-no people. (d) TF scenario 2-no people.

TABLE VI  
DECORRELATION DISTANCE OF DIFFERENT BUILDINGS

Building	Decorrelation distance
Office	2.8m
Residential Building	1.6m
Car park	1.8m
Warehouse	2.4m

as defined in Section III-A3, are calculated for each measurement track individually. As shown in Table VI, decorrelation distances varied between 1.6 and 2.8 m in different buildings. These are comparable with decorrelation distances in the order of 1–2 m reported in [20] for indoor measurements at 1800 and 5200 MHz. The results indicate that the LSF is almost independent from one local area to another.

### C. Summary of This Section

From the results in this section, we have the following findings.

- 1) The one slope PL model can be used to predict the PL in indoor environment, but it can only be used as a first-order prediction.
- 2) An AF model is required if we want to achieve more precise PL estimation in a multifloor building. Moreover, a site-specific model should be considered for each building as the construction materials, layout, as well as other factors will influence the PL greatly.
- 3) The decorrelation distance in a multifloor building is short which indicates that the LSF is almost independent from one local area to another.

## V. TEMPORAL FADING RESULTS

This section discusses the TF measurements of the indoor environment. Take office building as an example, Fig. 5 presents a series of typical TF samples of received power measured in TF scenarios 1 and 2, respectively. It can be seen in Fig. 5(a) that fades occur during the period of 0–110 s and 280–330 s, separated by periods during which the received signal strength remained almost constant. Clearly, the variations are caused by the movement of personnel in the laboratory. The typical dynamic range for fading in TF scenario 1 is found to be about 8 dB, and can be up to 17 dB occasionally. However, the TF measurements in TF scenario 2 are somewhat different [Fig. 5(b)]. Here, the received signal strength

TABLE VII  
RICIAN K-FACTOR PER BUILDING

Building	Moment-based		Curve fitting	
	TF 1	TF 2	TF 1	TF 2
Office Building	18.91	12.07	18.83	12.06
Residential Building	18.62	23.15	18.64	23.16
Car park	22.64	11.14	22.65	11.12
Warehouse	17.6	21.43	17.61	21.44

exhibits more variations, and is over a large dynamic range (typically 20 dB). This is because in TF scenario 2, there are more people moving around.

In order to verify the variations are indeed caused by people, we conduct another experiment at weekend midnight when there are no people in the office building. From the results in Fig. 5(c) and (d), we can see that there are only 1–2 dBm variations when there is no people in the environment. In this case, the small variations are mainly caused by the environmental changes (e.g., temperature and airflow), hardware noise, and thermal effects [28].

We further calculate the Rician  $K$ -factor using the two methods mentioned early in Section III-B. After obtaining the Rician  $K$ -factor, we compute the CDF and PDF of the received signal power for each scenario in different buildings. In this step, we are interested in the periods during which the fading occurs. To this end, data collected during the quiescent periods between fading variations are removed from the original samples. This is achieved by using a threshold detection algorithm to determine when the fading periods occur.

Table VII lists all  $K$ -factors for TF scenarios 1 and 2 using the moment-based method and least-square curve fitting method. We find that these two methods obtain similar results in both scenarios. Take office building as an example, Fig. 6 plots the CDF and PDF of the fitted Rician distribution model. We also plot the fitted Rayleigh distribution for comparison. From the good agreement between both types of estimators as well as the good correspondence between empirical and fitted Rician model in Fig. 6, we can draw the conclusion that the indoor environment TF follows Rician distribution. Similar results are also reported in the previous studies but with different  $K$ -factors [19], [23]. For example, the study in [23] shows that the Rician  $K$ -factor varies from 6 to 12 dB in a typical office environment. In an industrial environment, the  $K$ -factors are found to vary greatly from 4 to 19 dB [19].

The  $K$ -factor for the Rician model which best fits experimental results can reasonably be considered to be determined by the extent to which motion in the building alters the

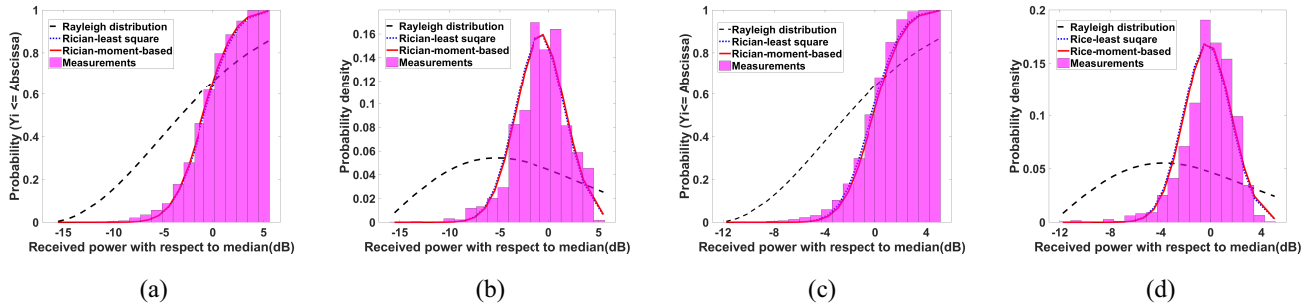


Fig. 6. CDF and PDF of fitted Rician distribution model. (a) CDF of scenario 1. (b) PDF of scenario 1. (c) CDF of scenario 2. (d) PDF of scenario 2.

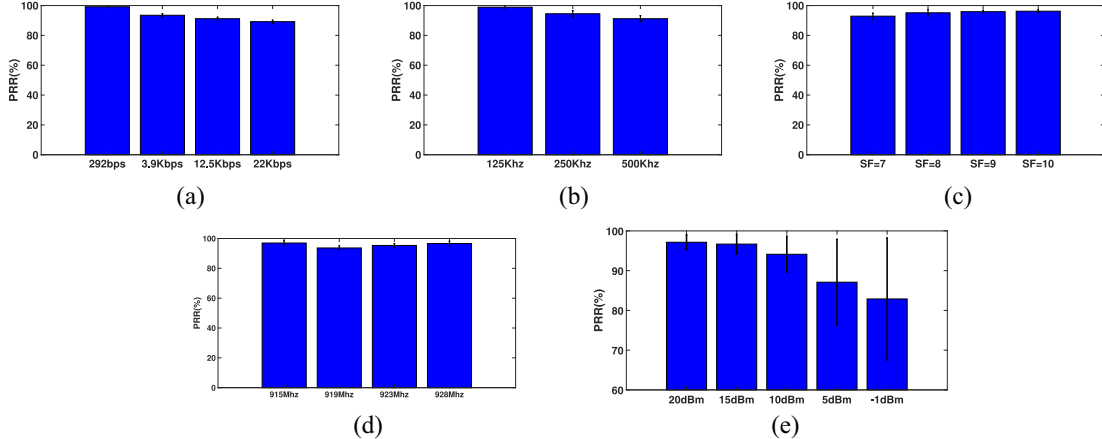


Fig. 7. Evaluation results of testbed. Impact of (a) data rate, (b) BW, (c) SF, (d) frequency, and (e) transmission power.

multipath structure at Rx. For example, in office building, the  $K$ -factor in scenario 2 is lower than that in scenario 1. As explained in Section III-B1, low  $K$ -factors indicate the large motion in the wireless propagation environment. This is because in scenario 2, Rx is put at the ground level where the entrance of building is located. Since there are more people moving around which leads to more variations in scenario 2. Similar patterns are also observed in other buildings. The lowest  $K$ -factor occurs in TF scenario 2 of car park where Rx is located near the exit of the car park. The frequent entrance and exit of cars causes large variations in the received power.

The obtained  $K$ -factors and the corresponding CDFs are used to calculate a fade margin associated with TF for a given outage probability. The outage probability, which determines the probability that the wireless system will be out of the service (quality of service not reached) and the corresponding fade margin will be used in the link budget calculation for the network planning applications. The details of the calculation are explained in [29]. For an outage probability of 0.01 (99% of the time, the variation around the median will not exceed the fade margin), the fade margin in different buildings is summarized in Table VIII. The fade margin can be used in link budget analysis.

#### A. Summary of This Section

Based on the results in this section, we have the following findings.

TABLE VIII  
FADE MARGIN IN DIFFERENT BUILDINGS

Building	Fade margin (dB)	
	TF scenario 1	TF scenario 2
Office Building	19.4	17.4
Residential Building	20.1	15
Car park	17.8	14.7
Warehouse	18.6	13.5

- 1) The moment-based method and least-square curve fitting method achieve similar results in terms of  $K$ -factor estimation.
- 2) TF is found to follow Rician distribution and Rician  $K$ -factors varies between 12 and 18 dB.
- 3) A fade margin of 9 dB in scenario 1 and 7 dB in scenario 2 can be considered in the link budget analysis.

## VI. COVERAGE EXPERIMENT RESULTS

### A. Coverage Analysis

1) *Results of Office Building:* Fig. 7 plots the evaluation results with average values and 95% confidence level. In the following, we analyze the impact of data rate, SF, BW, and frequency in turn.

Fig. 7(a) shows the PRR using different data rate. We notice that the higher the data rate is, the lower the PRR is. For example, the data rate of 292 b/s achieves the best PRR while the highest data rate (i.e., 22 kb/s) has the lowest PRR. This results correspond to the LoRa characteristics: a lower data rate has

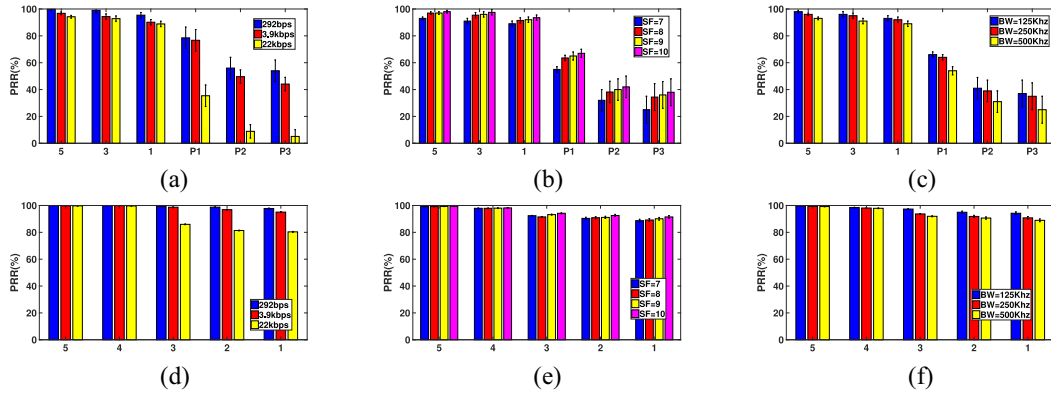


Fig. 8. Evaluation results of residential building (building 2) and car park (building 3). Impact of (a) data rate (building 2), (b) SF (building 2), (c) BW (building 2), (d) data rate (building 3), (e) SF (building 3), and (f) BW (building 3).

TABLE IX  
ENERGY CONSUMPTION (MJ)

BW	SF=7		SF=8		SF=9		SF=10	
	125Khz	500Khz	125Khz	500Khz	125Khz	500Khz	125Khz	500Khz
Data rate	5468 bps	21875 bps	3125 bps	12500 bps	1757 bps	7031 bps	976 bps	3906 bps
20dBm	9.36	0.33	10.22	0.342	10.24	0.57	11.98	1.02
15dBm	1.29	0.018	1.47	0.0294	1.66	0.059	1.91	0.105
10dBm	0.84	0.0059	0.86	0.0116	0.91	0.024	0.96	0.0421
5dBm	0.55	0.0055	0.57	0.0114	0.61	0.0204	0.65	0.0407
1dBm	0.43	0.0053	0.47	0.0108	0.53	0.0195	0.54	0.0341

stronger penetration ability and can achieve a longer communication distance. Followed by that Fig. 7(b) plots the impact of BW on PRR. We find that the greater the BW is, the lower PRR it achieves. This result corresponds well with the results in [30]. This is because the symbol rate  $R_s = (BW/2^{SF})$ ; therefore, when the transmission power is constant, the wider the BW is, the less energy will be distributed for each symbol. From Fig. 7(c), we find the PRR increases slightly when SF increases from 7 to 10. The reason is the same: when the transmission power is constant, the larger the SF is, the more energy will be distributed for each symbol.

The PRR of different center frequencies is plotted in Fig. 7(d). It can be seen that the PRR of channel 919 MHz is slightly lower than the other channels. This may be caused by the following reasons: it can be due to the different antenna efficiency or amplification gains for the frequencies, due to the interference from the environment, or due to the differences in the RF propagation for this frequency.

2) *Impact of Network Size:* As our testbed only consists of a limited number of LoRa nodes (e.g., 10), we use these nodes to emulate a higher number of nodes based on their duty cycle. In this experiment, we emulate up to 3000 nodes by changing the duty cycle following the method in [31]. Then, we evaluate the PRR of the network by changing SF. The other parameters are set to the default parameters in Table II. For each SF, the nodes were programmed to transmit packets randomly for 30 min. The results of different SF and different network size are shown in Fig. 9. Intuitively, the PRR of the whole network decreases when the number of nodes increases. However, we observe different patterns for SF. For example,

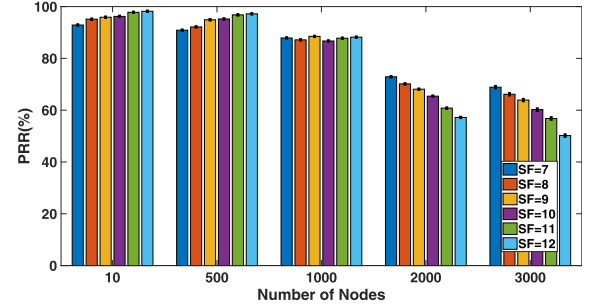


Fig. 9. Impact of network size.

when the network size is not large, the larger the SF is, the higher PRR it can achieve. When there are more nodes in the network, the larger the SF is, the lower PRR it can reach. The reasons are as follows as explained in [31]: smaller SF will lead to shorter airtime which means it will transmit more packets during the same time period. When the network size is not large, this might not be an issue. However, when the network size increases, it will increase the chances of collision as a large number of nonorthogonal transmissions use the same physical channel.

3) *Results of Residential Building and Car Park:* The results of residential building and car park are shown in Fig. 8. We can see that the impact of data rate, SF, and BW in these two buildings are the same as observed in office building. For example, the data rate of 292 b/s consistently achieves the best PRR across all the floors while the highest data rate (i.e., 22 kb/s) has the lowest PRR in these two buildings. Another

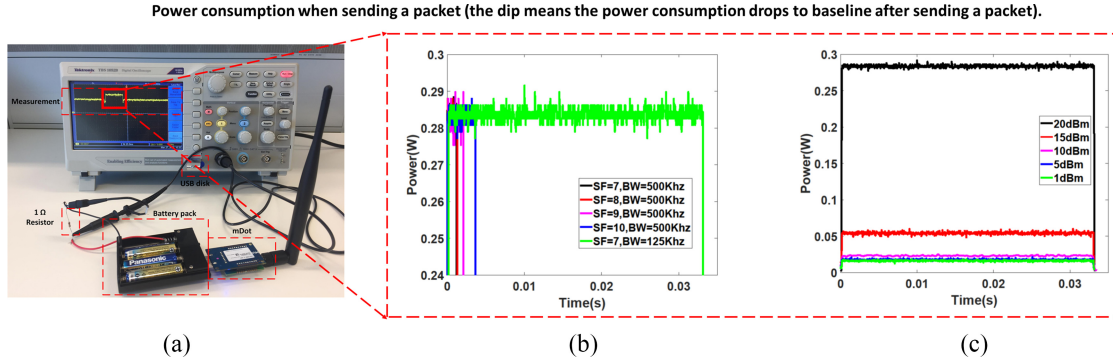


Fig. 10. Energy consumption profile. (a) Measurement setup. (b) Impact of different data rate. (c) Impact of different Tx power.

finding is that in the residential building, the PRR in basement P1–P3 is significantly lower than that of the levels above ground which suggests underground is indeed a challenging communication environment.

### B. Energy Consumption Analysis

In this section, we analyze the energy consumption of different communication settings. The experimental setup for the power measurement is shown in Fig. 10. In order to capture both the average current and time requirements for each transmission event, the Tektronix TBS1052B oscilloscope is used. As shown in the figure, we connect the mDot with a 1- $\Omega$  resistor in series and power it using a 4.5-V AA battery pack. The oscilloscope probe is then connected across the resistor to measure the current going through. The node keeps sending a 16-byte packet every 1 s using different SF, BW, and transmit power. The power consumption profile is stored in a USB disk for further analysis.

The SF and BW determine the data rate which further determines the on-air time and consequently the amount of the energy consumed to send a packet. Table IX summarizes the energy consumption under different parameter settings. From the results, we have the following two findings. First, when the node is transmitting at a constant data rate, there is a significant gap between the maximum transmitting power and others. For example, when using 976 b/s (SF = 10 and BW = 125 KHz) it consumes 11.98 mJ to transmit a 16-byte packet while it only consumes 1.91 mJ using 15-dBm transmitting power which means it consumes 6× less energy. Second, when the transmission power is constant, the energy consumption using the minimum data rate is remarkably higher than using the maximum data rate. For example, when using 10-dBm transmitting power, the energy consumption using the minimum data rate (SF = 10 and BW = 125 KHz) is 0.86 mJ which is 145× higher than that using the maximum data rate (SF = 7 and BW = 500 KHz) which is only 0.0059 mJ.

To provide an easier interpretation of the results, we plot the energy consumption profile in Fig. 10. We can see that the transmission time significantly increases with the decrease of data rate. Therefore, the low data rate will lead to longer on-air time and consequently consumes more energy. Also, it can be seen that the amount of energy consumed for sending the same packet using the minimum and the maximum transmit

power differs by 17×. The results emphasize the significance of choosing an appropriate transmission power and enabling the LoRa adaptive data rate feature in the energy-constrained applications.

### C. Application of the Results

Now, we illustrate how we can apply our findings in a real-world problem. Suppose, we want to deploy a sustainable gas meter network in a three-level building. Each sensor node is powered by an 800 mAh (8640 J) battery and the node requires to send 500 reliable measurements (8000 bytes) every 5 min. As it is a three-level building, from the results in Fig. 7(e), we can see that it can achieve over 90% PRR using 10-dBm transmission power. In this application, the transmission of 8000-byte data every 5 min requires a minimum data rate of 213 b/s. Therefore, all the data rates in the Table IX satisfy this requirement. As the smart gas meter network must be sustainable, we choose the maximum data rate which results in the least energy consumption. Therefore, the best solution for this application is using Tx power = 10 dBm, SF = 7, and BW = 500 KHz. Moreover, the results in Sections IV and V can be used as a guideline for network design. For example, suppose the sensitivity of the LoRa node is -120 dB, based on the results in Section IV, we can estimate that the RSSI will drop below -120 dB when Tx and Rx are separated by seven floors. The results in Section V such as fade margin can be used in the link budget calculation for the network planning applications.

## VII. RELATED WORK

This section discusses the previous studies that have been conducted to evaluate the performance or improve the performance of the LoRa technology. We categorize the previous studies into the following three groups based on their evaluation methods: 1) outdoor evaluation; 2) indoor evaluation; and 3) simulation.

### A. Outdoor Evaluation

As LoRaWAN aims at long distance wide-area network, researchers have conducted extensive tests in wide area outdoor environment to understand the performance and limitation of LoRaWAN. For example, Augustin *et al.* [8] provided a

TABLE X  
COMPARISON OF DIFFERENT WORKS

	[5]	[32]	[33]	[34]	[35]	[36]	[37]	Our work
Free space model One-slope model	Propagation Model	Free space model One-slope model Multi-wall model Multi-floor model	One-slope model	ITU One-slope model Multi-wall Ray tracing	×	One-slope model	ITM model	Free space model One-slope model Multi-wall model Multi-floor model
Environment	Outdoor	Indoor Outdoor	Outdoor	Indoor	Indoor	Indoor	Outdoor	Indoor
Temporal fading Model	×	×	×	×	×	✓	×	✓
Impact of network size	×	×	×	×	×	×	×	✓
Energy profile	×	×	×	×	×	×	×	✓
Coverage	✓	✓	✓	×	×	×	×	✓

comprehensive understanding of the LoRa modulation, including the data rate, frame format, spreading factor, receiver sensitivity, etc. The field tests show that LoRa can offer satisfactory network coverage up to 3 km in a suburban area with dense residential dwellings. Bor *et al.* [38] studied the range of reliable links, the receiver sensitivity, as well as LoRa scalability. They find that a typical smart city deployment can support 120 nodes per 3.8 ha, which is not sufficient for future IoT deployments. Also, LoRa networks can scale quite well if they use dynamic communication parameter selection and/or multiple sinks. In a similar work [1], the researchers analyze packet payloads, radio-signal quality, and spatiotemporal aspects, to model and estimate the performance of LoRaWAN. They also use their empirical findings in simulations to estimate the packet loss. Petajajarvi *et al.* [5] studied the coverage of LoRaWAN in a wide area. The measurements are conducted over the ground (using a car) and over the water (using a boat). An attenuation model for long-distance outdoor environment is also built based on the measurements. In recent work, researchers even study the channel characterization of LoRa in the Antarctic [7]. They find that varying terrain elevation is the dominating factor influencing the propagation in the Antarctic. Liando *et al.* [31] also conducted extensive evaluations based on a campus testbed which consists of 50 LoRa nodes. Their results show that in the LOS environment, the communication distance of LoRa can be over 10 km. However, under NLOS environments, the performance is severely affected by obstructions such as buildings.

### B. Indoor Evaluation

The characteristics and performance of LoRa technology in indoor buildings also received much research attention. Neumann *et al.* [39] studied the performance of LoRaWAN unconfirmed uplink data frames in an indoor environment. They showed that the ISM band duty cycle regulation limits the maximum amount of data that can be sent per day. They also evaluated the signal quality received from different locations to verify the feasibility of using LoRaWAN technology to cover an entire building. In another work, Cattani *et al.* [40] focused their evaluation on the impact of physical layer settings on the effective data rate and energy efficiency of communications. They found that it is often not worth tuning parameters, thereby reducing the data rate

in order to maximize the probability of successful reception, especially on links at the edge of their communication range. Moreover, they studied the impact of environmental factors on the performance of LoRa, and showed that higher temperatures significantly decrease the received signal strength and may remarkably affect packet reception. Similar to this article, Gregora *et al.* [35] also measured the indoor signal propagation characteristics of the LoRa technology in a building. However, their measurement is relatively simple and can just provide a rough understanding of signal propagation in a building. In another similar work, Benissa *et al.* [36] investigated the PL and TF of LoRa mote in dairy barns.

### C. Simulation

Simulation is a useful tool to understand the performance of the wireless network as field test takes too much effort and a large testbed in the real environment is not always available. For instance, Adelantado *et al.* [41] investigated the limitation of LoRaWAN via simulation and pointed out several open research challenges. Ferre *et al.* [42] studied the collision and packet loss of the LoRaWAN network via theoretical analysis. Because the LoRa technology is patented, only a few details about its operations are actually available. Many researchers have tried to reverse engineering the technology using software-defined radio (SDR) and they have successfully used SDR to encode/decode LoRa signal [43], [44]. In order to further extend the communication range of LoRa, researchers have investigated the LoRa backscatter system such as the work in [45] and [46].

In order to make the difference between this article and other works clearer, we provide a detailed comparison in Table X. Our studies differ from the previous works in the following two aspects. First, most field studies [1], [8], [31] were conducted in the outdoor environment because LoRa is originally designed for a wide-area network. Compared to these studies, the focus of this article is studying the performance of LoRa in multifloor buildings (e.g., indoor environment). Therefore, this article can be viewed as complementary work to previous studies. Second, although there exist several works that study the indoor signal propagation characteristics of LoRa, such as [35] and [36], their measurements are relatively simple and can just provide a rough understanding of signal propagation in a building. Compared to these works, we not only perform a detailed study to understand the performance

of different communication parameters in an indoor building but also study the characteristics of LSF and TF. Additionally, we validate our results by employing a small testbed and emulation.

### VIII. CONCLUSION

Understanding the performance and characterization of the LoRa technology in indoor buildings is imperative for its deployment and application. In this article, we have presented a comprehensive and sophisticated study regarding the LSF characteristics, TF characteristics, and coverage of the LoRa technology in four types of multifloor buildings, as well as energy consumption using different communication modes. We hope the findings presented in this article can also provide insights into the development of practical LoRa-based indoor applications.

### REFERENCES

- [1] N. Blenn and F. Kuipers, "LoRaWAN in the wild: Measurements from the things network," *arXiv preprint arXiv:1706.03086*, 2017.
- [2] *LoRa*. Accessed: Oct. 31, 2019. [Online]. Available: <https://www.lora-alliance.org>
- [3] *Sigfox*. Accessed: Oct. 31, 2019. [Online]. Available: <https://www.sigfox.com/en>
- [4] *NBLoT*. Accessed: Oct. 31, 2019. [Online]. Available: <https://www.u-blox.com/en/narrowband-iot-nb-iot>
- [5] J. Petajajarvi, K. Mikhaylov, A. Roivainen, T. Hanninen, and M. Pettissalo, "On the coverage of LPWANs: Range evaluation and channel attenuation model for LoRa technology," in *Proc. 14th Int. Conf. ITS Telecommun. (ITST)*, 2015, pp. 55–59.
- [6] S. Kartakis, B. D. Choudhary, A. D. Gluhak, L. Lambrinos, and J. A. McCann, "Demystifying low-power wide-area communications for city IoT applications," in *Proc. 10th ACM Int. Workshop Wireless Netw. Testbeds Exp. Eval. Characterization*, 2016, pp. 2–8.
- [7] J. Gaelens, P. Van Torre, J. Verhaevert, and H. Rogier, "LoRa mobile-to-base-station channel characterization in the Antarctic," *Sensors*, vol. 17, no. 8, p. 1903, 2017.
- [8] A. Augustin, J. Yi, T. Clausen, and W. M. Townsley, "A study of LoRa: Long range & low power networks for the Internet of Things," *Sensors*, vol. 16, no. 9, p. 1466, 2016.
- [9] J. Haxhibeqiri, I. Moerman, and J. Hoebeke, "Low overhead scheduling of LoRa transmissions for improved scalability," *IEEE Internet Things J.*, vol. 6, no. 2, pp. 3097–3109, Apr. 2019.
- [10] Y. Okumura, "Field strength and its variability in VHF and UHF land-mobile radio service," *Rev. Electr. Commun. Lab.*, vol. 16, pp. 825–873, 1968.
- [11] V. Erceg *et al.*, "An empirically based path loss model for wireless channels in suburban environments," *IEEE J. Sel. Areas Commun.*, vol. 17, no. 7, pp. 1205–1211, Jul. 1999.
- [12] P. Series, "Propagation data and prediction methods for the planning of indoor radiocommunication systems and radio local area networks in the frequency range 900 MHz to 100 GHz," Int. Telecommun. Union, Geneva, Switzerland, ITU-Recommendation 1238-7, 2012.
- [13] A. H. Ali, M. R. A. Razak, M. Hidayah, S. A. Azman, M. Z. M. Jasmin, and M. A. Zainol, "Investigation of indoor WiFi radio signal propagation," in *Proc. IEEE Symp. Ind. Electron. Appl. (ISIEA)*, 2010, pp. 117–119.
- [14] W. Li, X. Hu, and T. Jiang, "Path loss models for IEEE 802.15.4 vehicle-to-infrastructure communications in rural areas," *IEEE Internet Things J.*, vol. 5, no. 5, pp. 3865–3875, Oct. 2018.
- [15] A. I. Sulyman, A. T. Nassar, M. K. Samimi, G. R. MacCartney, T. S. Rappaport, and A. Alsanie, "Radio propagation path loss models for 5G cellular networks in the 28 GHz and 38 GHz millimeter-wave bands," *IEEE Commun. Mag.*, vol. 52, no. 9, pp. 78–86, Sep. 2014.
- [16] S. Benissa *et al.*, "Experimental characterisation of the off-body wireless channel at 2.4 GHz for dairy cows in barns and pastures," *Comput. Elect. Agricult.*, vol. 127, pp. 593–605, Sep. 2016.
- [17] T. S. Rappaport *et al.*, *Wireless Communications: Principles and Practice*, vol. 2. Upper Saddle River, NJ, USA: Prentice-Hall, 1996.
- [18] A. Aragon-Zavala, *Antennas and Propagation for Wireless Communication Systems*. Hoboken, NJ, USA: Wiley, 2008.
- [19] E. Tanghe *et al.*, "The industrial indoor channel: Large-scale and temporal fading at 900, 2400, and 5200 MHz," *IEEE Trans. Wireless Commun.*, vol. 7, no. 7, pp. 2740–2751, Jul. 2008.
- [20] N. Jaldén, P. Zetterberg, B. Ottersten, A. Hong, and R. Thoma, "Correlation properties of large scale fading based on indoor measurements," in *Proc. Wireless Commun. Netw. Conf. WCNC*, 2007, pp. 1894–1899.
- [21] J. D. Parsons, *The Mobile Radio Propagation Channel*. London, U.K.: Pentech Press, 1992.
- [22] A. Abdi, C. Tepedelenlioglu, M. Kaveh, and G. Giannakis, "On the estimation of the K parameter for the Rice fading distribution," *IEEE Commun. Lett.*, vol. 5, no. 3, pp. 92–94, Mar. 2001.
- [23] S. Y. Seidel and T. S. Rappaport, "914 MHz path loss prediction models for indoor wireless communications in multifloored buildings," *IEEE Trans. Antennas Propag.*, vol. 40, no. 2, pp. 207–217, Feb. 1992.
- [24] H. K. Rath, S. Timmadasari, B. Panigrahi, and A. Simha, "Realistic indoor path loss modeling for regular WiFi operations in India," in *Proc. 23rd Nat. Conf. Commun. (NCC)*, 2017, pp. 1–6.
- [25] J. Keenan, "Radio coverage in buildings," *Brit. Telecom Technol. J.*, vol. 8, no. 1, pp. 19–24, 1990.
- [26] A. J. Motley and J. M. P. Keenan, "Personal communication radio coverage in buildings at 900 MHz and 1700 MHz," *Electron. Lett.*, vol. 24, no. 12, pp. 763–764, 1988.
- [27] C. R. Anderson and T. S. Rappaport, "In-building wideband partition loss measurements at 2.5 and 60 GHz," *IEEE Trans. Wireless Commun.*, vol. 3, no. 3, pp. 922–928, May 2004.
- [28] S. Jana, S. N. Premnath, M. Clark, S. K. Kasera, N. Patwari, and S. V. Krishnamurthy, "On the effectiveness of secret key extraction from wireless signal strength in real environments," in *Proc. 15th Annu. Int. Conf. Mobile Comput. Netw.*, 2009, pp. 321–332.
- [29] A. Goldsmith, *Wireless Communications*. New York, NY, USA: Cambridge Univ. Press, 2005.
- [30] J. Petäjäjärvi, K. Mikhaylov, R. Yasmin, M. Hääläinen, and J. Iinatti, "Evaluation of LoRa LPWAN technology for indoor remote health and wellbeing monitoring," *Int. J. Wireless Inf. Netw.*, vol. 24, no. 2, pp. 153–165, 2017.
- [31] J. C. Liando, A. Gamage, A. W. Tengourtius, and M. Li, "Known and unknown facts of LoRa: Experiences from a large-scale measurement study," *ACM Trans. Sensor Netw.*, vol. 15, no. 2, p. 16, 2019.
- [32] R. El Chall, S. Lahoud, and M. El Helou, "LoRaWAN network: Radio propagation models and performance evaluation in various environments in Lebanon," *IEEE Internet Things J.*, vol. 6, no. 2, pp. 2366–2378, Apr. 2019.
- [33] P. Jörke, S. Böcker, F. Liedmann, and C. Wietfeld, "Urban channel models for smart city IoT-networks based on empirical measurements of LoRa-links at 433 and 868 MHz," in *Proc. IEEE 28th Annu. Int. Symp. Pers. Indoor Mobile Radio Commun. (PIMRC)*, 2017, pp. 1–6.
- [34] S. Hosseini-zadeh, H. Larjani, K. Curtis, A. Wixted, and A. Amini, "Empirical propagation performance evaluation of LoRa for indoor environment," in *Proc. IEEE 15th Int. Conf. Ind. Informat. (INDIN)*, 2017, pp. 26–31.
- [35] L. Gregora, L. Vojtech, and M. Neruda, "Indoor signal propagation of LoRa technology," in *Proc. 17th Int. Conf. Mechatronics Mechatronika*, 2016, pp. 1–4.
- [36] S. Benissa *et al.*, "Internet of animals: Characterisation of LoRa sub-GHz off-body wireless channel in dairy barns," *Electron. Lett.*, vol. 53, no. 18, pp. 1281–1283, 2017.
- [37] H. Linka, M. Rademacher, O. G. Aliu, and K. Jonas, "Path loss models for low-power wide-area networks: Experimental results using LoRa," 2018.
- [38] M. C. Bor, U. Roedig, T. Voigt, and J. M. Alonso, "Do LoRa low-power wide-area networks scale?" in *Proc. 19th ACM Int. Conf. Model. Anal. Simulat. Wireless Mobile Syst.*, 2016, pp. 59–67.
- [39] P. Neumann, J. Montavont, and T. Noël, "Indoor deployment of low-power wide area networks (LPWAN): A LoRaWAN case study," in *Proc. IEEE 12th Int. Conf. Wireless Mobile Comput. Netw. Commun. (WiMob)*, 2016, pp. 1–8.
- [40] M. Cattani, C. A. Boano, and K. Römer, "An experimental evaluation of the reliability of LoRa long-range low-power wireless communication," *J. Sensor Actuator Netw.*, vol. 6, no. 2, p. 7, 2017.
- [41] F. Adelantado, X. Vilajosana, P. Tuset-Peiro, B. Martinez, J. Melia-Segui, and T. Watteyne, "Understanding the limits of LoRaWAN," *IEEE Commun. Mag.*, vol. 55, no. 9, pp. 34–40, Sep. 2017.

- [42] G. Ferre, "Collision and packet loss analysis in a LoRaWAN network," in *Proc. 25th Eur. Signal Process. Conf. (EUSIPCO)*, 2017, pp. 2586–2590.
- [43] *DecodingLoRa*. Accessed: Oct. 31, 2019. [Online]. Available: <http://revspace.nl/DecodingLora/>
- [44] *LoRaSDR*. Accessed: Oct. 31, 2019. [Online]. Available: <http://github.com/myriadrf/LoRa-SDR/>
- [45] V. Talla, M. Hessar, B. Kellogg, A. Najafi, J. R. Smith, and S. Gollakota, "LoRa backscatter: Enabling the vision of ubiquitous connectivity," *Proc. ACM Interact. Mobile Wearable Ubiquitous Technol.*, vol. 1, no. 3, p. 105, 2017.
- [46] Y. Peng *et al.*, "PLoRa: A passive long-range data network from ambient LoRa transmissions," in *Proc. Conf. ACM Special Interest Group Data Commun.*, 2018, pp. 147–160.



**Weitao Xu** (GS'16–M'17) received the B.E. degree in communication engineering and the M.E. degree in communication and information system from the School of Information Science and Engineering, Shandong University, Jinan, China, in 2010 and 2013, respectively, and the Ph.D. degree from the University of Queensland, Brisbane, QLD, Australia, in 2017, under the supervision of Prof. N. Bergmann and Dr. W. Hu.

He is an Assistant Professor with the Department of Computer Science, City University of Hong Kong, Hong Kong. He was a Post-Doctoral Research Associate with the School of Computer Science and Engineering, University of New South Wales, Sydney, NSW, Australia, from June 2017 to August 2019.

Prof. Xu is a member of ACM.



**Jun Young Kim** (GS'14) received the Ph.D. degree from the University of New South Wales, Sydney, NSW, Australia, in 2017.

He is currently leading the Research and Development Team, WBS Technology, Sydney, to develop a smart building service. His current research interest includes security and management of the Internet of Things.



**Walter Huang** is the Director of WBS Technology, Sydney, NSW, Australia. WBS Technology is recognized as Australia's leading manufacturer of high quality LED Emergency Lighting, LED Exit Signs and LED Lighting Systems. At WBS, we have a holistic approach to your lighting system requirements and combined with our "affordable quality" energy efficient lighting products gives us a fantastic opportunity to work together with you to achieve a significant savings to your bottom line.



**Salil S. Kanhere** received the M.S. and Ph.D. degrees in electrical engineering from Drexel University, Philadelphia, PA, USA, in 2001 and 2003, respectively.

He is currently a Professor with the School of Computer Science and Engineering, University of New South Wales, Sydney, NSW, Australia. He is currently a Contributing Research Staff with the National ICT Australia, Sydney, and a Faculty Associate with the Institute for Infocomm Research, Singapore. His current research interests include pervasive computing, crowdsourcing, embedded sensor networks, mobile networking, privacy, and security. He has authored/coauthored over 140 peer-reviewed articles and delivered over 15 tutorials and keynote talks in the above areas.

Prof. Kanhere was a recipient of the Humboldt Research Fellowship in 2014. He regularly serves on the organizing committee of a number of IEEE and ACM international conferences, such as the IEEE PerCom, ACM MobiSys, ACM SenSys, ACM CoNext, the IEEE WoWMoM, the IEEE LCN, ACM MSWiM, the IEEE DCOSS, the IEEE SenseApp, ICDCN, and ISSNIP. He currently serves as an Area Editor for *Pervasive and Mobile Computing, Computer Communications, the International Journal of Ad Hoc, and Ubiquitous Computing and Mobile Information Systems*.



**Sanjay K. Jha** (SM'08) received the Ph.D. degree from the University of Technology Sydney, Ultimo, NSW, Australia.

He is a Professor, the Head of the Networked Systems and Security Group, and the Director of CySPri Laboratory, School of Computer Science and Engineering, University of New South Wales, Sydney, NSW, Australia. He has published over 180 articles in high quality journals and conferences. His current research interests include networking including wireless sensor networks, ad hoc/community wireless networks, resilience and multicasting in IP networks, and security protocols for wired/wireless networks.



**Wen Hu** (S'04–M'06–SM'12) received the Ph.D. degree from the University of New South Wales, Sydney, NSW, Australia, in 2004.

He is an Associate Professor with the School of Computer Science and Engineering, University of New South Wales, Sydney, NSW, Australia. His current research interests include novel applications, low power communications, security and compressive sensing in sensor network systems, and Internet of Things.